

Frequency shifts in NIST Cs primary frequency standards due to transverse rf field gradientsNeil Ashby,^{*} Stephan Barlow,[†] Thomas Heavner,[‡] and Steven Jefferts[§]
National Institute of Standards and Technology, Boulder, Colorado 80305, USA

(Received 29 October 2014; published 23 March 2015)

A single-particle Green's function (propagator) is introduced to study the deflection of laser-cooled cesium atoms in an atomic fountain due to microwave magnetic field gradients in the Ramsey TE₀₁₁ cavity. The deflection results in a state-dependent loss of atoms at apertures in the physics package, resulting in a frequency bias. A model accounting only for motion in one dimension transverse to the symmetry axis of the fountain is discussed in detail and then generalized to two transverse dimensions. Results for fractional frequency shifts due to transverse field gradients are computed for NIST-F1 and NIST-F2 cesium fountains. The shifts are found to be negligible except in cases of higher rf power applied to the cavities.

DOI: [10.1103/PhysRevA.91.033624](https://doi.org/10.1103/PhysRevA.91.033624)

PACS number(s): 03.75.Dg, 06.20.fb, 06.30.Ft

I. INTRODUCTION

Frequency shifts in atomic clocks are of fundamental importance in the accuracy determination of the SI second, which is presently realized using laser-cooled Cs fountains operated by many standards laboratories around the world [1]. The potential systematic bias due to momentum-changing interactions between the microwave interrogation field and the atoms undergoing Ramsey excitation have long been a source of concern, investigation, and conjecture. Bordé and Wolf estimated the fractional frequency shift due to microwave recoil in atomic standards to be on the order of $\frac{\delta f}{f} \approx 10^{-16}$ [2].

Recently, Gibble [3,4] published a theory reinvestigating the microwave recoil shift along lines originally used by Cook [5,6]. Reference [4] uses Cook's methods in the optical domain to quantify the state-dependent deflection in the atomic trajectories due to gradients in the microwave field and the resulting frequency bias. This work contains several results we find to be unphysical and predicts a frequency shift of order 10^{-16} [4]; several primary frequency standard groups (NPL, PTB, SYRTE) are correcting for this bias while NIST and INFN are not. Here we present an alternate theoretical treatment that extends the work by Cook or Gibble.

The operation of the NIST fountains has been described in Ref. [7]. Figure 1 shows a simplified configuration of the NIST-F1 cesium fountain. A cloud of atoms is collected and laser cooled to $\approx 0.5 \mu\text{K}$ in optical molasses, then launched upwards through a state-selection region that results in a sample of atoms in the $|F, m_F\rangle = |3, 0\rangle$ state. The atoms pass into a Ramsey cavity (a cylindrical TE₀₁₁ cavity), where they are subject to a $\pi/2$ pulse of resonant rf (radio frequency) radiation of frequency $f_0 = 9.192631770 \text{ GHz}$ that puts the atoms into a superposition of the two clock states $|4, 0\rangle$ and $|3, 0\rangle$. The atoms then coast upwards into a drift region and fall back down through the cavity where they are subjected to a second $\pi/2$ pulse. This causes some of the atoms to make transitions to the upper hyperfine state. The atoms then fall through a detection region that measures the numbers of

atoms in each state; from the detected atom numbers in the two hyperfine states a relative transition probability is measured.

Here we use a full wave-packet description of the atoms undergoing Ramsey excitation along with a full time-dependent solution to the Schrödinger equation that propagates the wave packets through the two microwave interactions up through the detection step. We find frequency shifts of order 10^{-17} in our atomic fountains [7] with our theory. (Because the microwave cavity is essentially identical in the two fountains at NIST and the geometry of the standards is similar, the results given here are representative of those for both fountains.)

The organization of this paper is as follows. In Sec. II we introduce the Schrödinger equation for a two-state model of the hyperfine states of ¹³³Cs, coupled to the axial component of the rf magnetic field in a cylindrically symmetric cavity. The Hamiltonian of this problem includes kinetic energy, internal energy of the hyperfine states, and magnetic interaction energy of the spins with the magnetic field. The rf field is assumed to be almost exactly resonant, a slight detuning is modeled by allowing the phase of the rf field to be different when the atoms pass through the cavity a second time. In the presence of transverse microwave magnetic field gradients, which are dictated by vanishing of the transverse magnetic field at the cylindrical cavity boundaries, the transverse motion of the atoms is slightly affected. This is described by the introduction of a propagator that exactly solves the Schrödinger equations after they are decoupled by a series of exact transformations. We consider mainly the case of a $\pi/2$ pulse applied in each cavity but discuss up to $7\pi/2$ pulses in a later section. The propagator accounts for the transverse recoil of the atoms due to the interaction of the spins with the field gradients. Time development of the phases of the spinor components are discussed in Sec. III. Sections IV, V, and VI discuss construction of atom wave packets and their quantum-mechanical spreading during propagation through the apparatus. In Sec. VII a prototype one-dimension model of passage of a ball of laser-cooled atoms at temperature $T \approx 1 \mu\text{K}$, with spatial extent σ_n in the transverse dimension, is developed in detail and solutions of the Schrödinger equation for balls entering the detector are presented. Section VIII discusses the method of detection and Sec. IX describes results for the one-dimensional case. Section X generalizes the model to the full two-dimensional case of transverse motion. The results for this case are described in Sec. XI.

^{*}ashby@boulder.nist.gov[†]sbarlow@boulder.nist.gov[‡]heavner@boulder.nist.gov[§]jefferts@boulder.nist.gov

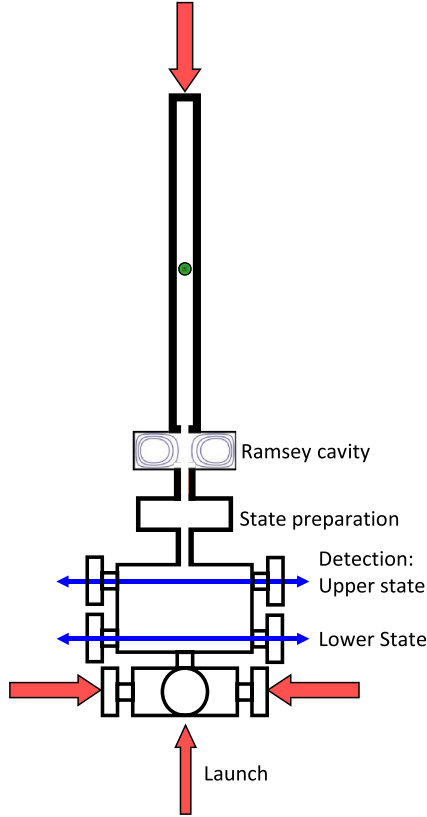


FIG. 1. (Color online) Schematic diagram of the main components of NIST-F2. See text for discussion.

II. EQUATIONS OF MOTION

In this section we derive decoupled equations of motion for the atoms in the fountain and introduce a propagator (Green's function) that solves the spatial equations of motion for the atoms in a transverse magnetic field gradient. The $\langle F, m_F | = \langle 4, 0 |$ and $\langle F, m_F | = \langle 3, 0 |$ hyperfine states of ^{133}Cs , of intrinsic energies $\hbar\omega_a$ and $\hbar\omega_b$, respectively, are coupled only by the z component of an applied microwave magnetic field [8]. We consider a two-state model in which the energy separation of the hyperfine states is $\hbar\Delta = \hbar(\omega_a - \omega_b)$ and the zero of energy is halfway in between ω_a and ω_b . ψ_a , and ψ_b denote the wave functions of atoms in the upper and lower hyperfine states, respectively. In the presence of an applied rf field the equations of motion are

$$i\hbar \frac{\partial \psi_a}{\partial t} = -\frac{\hbar^2}{2m} \nabla^2 \psi_a + \frac{\hbar\Delta}{2} \psi_a + \mu_B g B_z \psi_b; \quad (1)$$

$$i\hbar \frac{\partial \psi_b}{\partial t} = -\frac{\hbar^2}{2m} \nabla^2 \psi_b - \frac{\hbar\Delta}{2} \psi_b + \mu_B g B_z \psi_a. \quad (2)$$

For a TE_{011} mode in a cylindrical cavity the applied high-frequency rf field may be represented by

$$\begin{aligned} \mu_B g B_z &= \hbar\pi b \cos(\omega t + \theta_1) \\ &= \hbar\pi b_0 \cos(\omega t + \theta_1) J_0(x_1 r/d) \sin(Kz), \end{aligned} \quad (3)$$

where $K = (\omega^2/c^2 - x_1^2/d^2)^{1/2}$, b_0 is a conveniently chosen measure of the amplitude, $x_1 = 3.83171 \dots$ is the first zero of the ordinary Bessel function of order 1, d is the cavity radius,

and c is the speed of light. The applied field is assumed to be almost exactly on resonance: $\omega \approx \Delta$.

In NIST-F1 and NIST-F2, the symmetry axis of the cylindrical cavity is along the z direction. After entering the cavity at the reference level $z = 0$, atoms are subject to a half-sine wave pulse of rf energy [the $\sin(Kz)$ in Eq. (3)], coast upwards to height h above the cavity entrance, then fall back down through the cavity where another pulse is applied, then fall into a detector. We allow the phases of the rf fields during cavity passage to be different: θ_1 and θ_2 , respectively. Time of passage through the cavities is denoted by τ , time in the drift region by T , and time T_d to fall from the bottom of the cavity into the detector.

The cavity has entry and exit apertures of radius $r_a < d/2$, and an atom can enter the cavity at some off-axis position x_c, y_c where we think of this position as the center of a Gaussian wave packet whose spread is small compared to the scale of distance over which the microwave magnetic field changes in the transverse direction. A one-dimensional Gaussian wave packet initially centered at x_c can be constructed by superposing plane waves:

$$\begin{aligned} \phi(x, t) &= \sqrt{\frac{\sigma}{2\pi^{3/2}}} \int_{-\infty}^{\infty} dk e^{i(k(x-x_c) - \frac{\hbar k^2 t}{2m} - \sigma^2(k-k_0)^2/2)} \\ &= \frac{1}{\pi^{1/4}} \frac{e^{i(k_0(x-x_c) - \hbar k_0^2 t/(2m))}}{\sqrt{\sigma + i\hbar t/(\sigma m)}} e^{-\frac{(x-x_c - \hbar k_0 t/m)^2}{2(\sigma^2 + i\hbar t/m)}}, \end{aligned} \quad (4)$$

where $\hbar k_0/m$ is the central velocity of the packet. The wave packet of Eq. (4) is normalized to unity and satisfies the Schrödinger equation for a free particle,

$$i\hbar \frac{\partial \phi(x, t)}{\partial t} = -\frac{\hbar^2}{2m} \nabla^2 \phi(x, t). \quad (5)$$

Quantum-mechanical packet spreading occurs due to the terms proportional to $\hbar t/m$ in the denominators of Eq. (4).

It will be seen that all of the integrations performed as we follow the trajectory of an atom involve Gaussian exponentials; such integrals can be performed in any order and the packets are normalized by means of the weighting functions in Eq. (4), so it will be convenient to simply assume that the packet entering the first cavity can be represented by a plane wave at $t = 0$:

$$e^{i[k_x(x-x_c) + k_y(y-y_c)]}. \quad (6)$$

At an off-axis position x_c, y_c there is a transverse field gradient arising from the Bessel function in Eq. (3). Expanding in a Taylor series about such a position,

$$\begin{aligned} \hbar\pi b_0 J_0(x_1 r/d) &= \hbar\pi b_0 J_0(x_1 \sqrt{x_c^2 + y_c^2}/d) \\ &\quad + 2\gamma_x(x - x_c) + 2\gamma_y(y - y_c), \end{aligned} \quad (7)$$

where for example,

$$\gamma_x = \frac{\hbar\pi b_0}{2} \left. \frac{\partial J_0(x_1 r/d)}{\partial x} \right|_{x_c, y_c}. \quad (8)$$

These gradients exert transverse forces on the spins and result in transverse displacements that are, however, quite tiny, as will be seen. That the gradients occur as a sum of terms in $x - x_c$ and $y - y_c$ in the equations of motion, makes it possible to solve Eqs. (1) and (2) by separating variables.

The time dependence in the equations of motion is simplified by passing to the rotating-phase approximation. We introduce a transformation of functions by means of

$$\begin{bmatrix} \psi_a \\ \psi_b \end{bmatrix} = \begin{bmatrix} e^{-i(\omega t/2 + \theta_1/2)} D_a \\ e^{i(\omega t/2 + \theta_1/2)} D_b \end{bmatrix}. \quad (9)$$

Then introducing the exponential form for the $\cos(\omega t + \theta_1)$ appearing in Eq. (3) and neglecting terms that oscillate with twice the hyperfine resonance frequency, the equations of motion become

$$\begin{aligned} i\hbar \frac{\partial D_a}{\partial t} &= -\frac{\hbar^2}{2m} \nabla^2 D_a + \frac{\hbar\pi b}{2} D_b + \frac{\hbar(\Delta - \omega)}{2} D_a; \\ i\hbar \frac{\partial D_b}{\partial t} &= -\frac{\hbar^2}{2m} \nabla^2 D_b + \frac{\hbar\pi b}{2} D_a - \frac{\hbar(\Delta - \omega)}{2} D_b. \end{aligned} \quad (10)$$

We shall neglect the detuning terms in Eqs. (10) above. In the case where no spatial dependence is considered, it can be shown [9] that these terms cause a very small change in the width of the central Ramsey fringe; detuning does not itself cause a frequency shift. We shall however keep the exponential phase terms in Eq. (9) as they play an important role in the discussion of detection. The equations can then be decoupled by introducing the following linear combinations of wave functions:

$$f_+ = \frac{1}{\sqrt{2}}(D_a + D_b); \quad f_- = \frac{1}{\sqrt{2}}(D_a - D_b). \quad (11)$$

The equations of motion become:

$$i\hbar \frac{\partial f_{\pm}}{\partial t} = -\frac{\hbar^2}{2m} \nabla^2 f_{\pm} \pm \frac{\hbar\pi b}{2} f_{\pm}. \quad (12)$$

Such linear combinations were introduced by Cook [5] to treat motion of electric dipoles under the influence of a laser beam; the f_+ and f_- packets are displaced in opposite directions, but consist at all times of equal contributions from the a and b spinor states, but with different phases. The solution for f_- can be obtained from the f_+ solution by changing the sign of b , so we shall consider only the $+$ sign and for convenience will drop the subscript.

Launched atoms entering the cavity aperture arrive with a thermal distribution of velocities and hence with a distribution of arrival times; also the atom cloud may be clipped by the aperture edges. Passage of the cloud through the cavity may thus entail a distribution of positions within the aperture as well as a distribution of times τ required to pass through the cavity. We shall consider a particular packet centered at (x_c, y_c) with a velocity $\hbar\mathbf{k}/m$ on entry to the cavity. Transition probabilities for such an atom will be averaged over position and velocity at the end of the calculation. As the packet traverses the cavity, it samples the half-sine wave dependence of the resonant rf field; this field in effect becomes a slowly varying time-dependent field because the packet will be well localized compared to the cavity length. The packet falls back through the cavity some time later; we assume that the second time of passage is the same as that during the first passage. We therefore seek a reasonable approximation that allows description of the motion in the z direction to be separated off; effects of field gradients in the z direction cancel out and are not of interest in the present

paper. Therefore we assume

$$f(x, y, z, t) = u(x, y, t)\phi(z, t); \quad (13)$$

where $\phi(z, t)$ is of the general form of Eq. (4). Then Eq. (12) becomes

$$\phi(z, t) i\hbar \frac{\partial u}{\partial t} = -\frac{\hbar^2}{2m} \phi(z, t) \left(\frac{\partial^2 u}{\partial x^2} + \frac{\partial^2 u}{\partial y^2} \right) + \frac{\hbar\pi b}{2} \phi(z, t) u. \quad (14)$$

If we multiply by $\phi(z, t)^*$ the z dependence can be simplified since integrating over all z ,

$$\int |\phi(z, t)|^2 \sin(Kz) dz = \sin\left(\frac{K\hbar k_z t}{m}\right) \times e^{-\frac{\kappa^2 \hbar^2 k_z^2 t^2}{m^2} (\sigma^2 + \hbar^2 t^2 / (\sigma^2 m^2))}. \quad (15)$$

The quantity appearing in the exponent in Eq. (15) is extremely small during cavity passage and cannot affect the resonant frequency, so we shall neglect it and retain the time-dependent sine function. Eq. (14) then becomes

$$\begin{aligned} i\hbar \frac{\partial u}{\partial t} &= -\frac{\hbar^2}{2m} \left(\frac{\partial^2 u}{\partial x^2} + \frac{\partial^2 u}{\partial y^2} \right) \\ &+ \sin(\kappa t) \left(\frac{\hbar\pi b_1}{2} + \gamma_x(x - x_c) + \gamma_y(y - y_c) \right) u, \end{aligned} \quad (16)$$

where $b_1 = (\hbar\pi b_0/2) J_0(x_1 \sqrt{x_c^2 + y_c^2}/d)$, γ_x is given in Eq. (8) and where $\kappa = K\hbar k_0/m$. The first time-dependent term in Eq. (16) can be eliminated by letting [9]:

$$u(x, y, t) = e^{-ia(t)} w(x, y, t). \quad (17)$$

Then if

$$a(t) = \frac{\pi b_1}{2} \int_0^t \sin \kappa t' dt', \quad (18)$$

Eq. (16) reduces to

$$\begin{aligned} i\hbar \frac{\partial w}{\partial t} &= -\frac{\hbar^2}{2m} \left(\frac{\partial^2 w}{\partial x^2} + \frac{\partial^2 w}{\partial y^2} \right) \\ &+ \sin(\kappa t) (\gamma_x(x - x_c) + \gamma_y(y - y_c)) w. \end{aligned} \quad (19)$$

The quantities $a(t)$ represent phases arising from the near-axis values of the applied rf field and have nothing to do with the a, b labels on the hyperfine states. The effective Hamiltonian on the right of Eq. (19) is a sum of terms that permit a solution by separation of variables into a product of factors of similar form. If we let $w(x, y, t) = \alpha(x, t)\beta(y, t)$, then a solution of Eq. (19) is found if α satisfies

$$i\hbar \frac{\partial \alpha}{\partial t} = -\frac{\hbar^2}{2m} \frac{\partial^2 \alpha}{\partial x^2} + \gamma_x(x - x_c) \sin(\kappa t) \alpha, \quad (20)$$

with an equation of motion of similar form for $\beta(y, t)$. [There will be another set of solutions with opposite signs for $a(t)$ and γ_x , corresponding to selecting the “ $-$ ” option in Eq. (13).] We shall drop the subscript on γ_x as long as we are discussing a one-dimensional model.

Separation of variables usually involves a separation constant; in the present case this quantity becomes a function of

time. However its effect can be shown to cancel out of the product $\alpha(x,t)\beta(y,t)$.

At the boundary $z = 0$, we take $t = 0$ and require that the wave function be a plane wave. Then Eq. (20) can be solved with the propagator (Green's function)

$$G_\gamma(x,t;x',0) = \sqrt{\frac{m}{2\pi i\hbar t}} e^{iS/\hbar}, \quad (21)$$

where

$$S = \frac{m}{2t}(x-x')^2 - \frac{\gamma(x-x_c)}{\kappa} \left(-\cos(\kappa t) + \frac{\sin(\kappa t)}{\kappa t} \right) - \frac{\gamma(x'-x_c)}{\kappa} \left(1 - \frac{\sin(\kappa t)}{\kappa t} \right) - \gamma^2 \left(\frac{-2 + 2\kappa^2 t^2 + 2\cos(2\kappa t) + \kappa t \sin(2\kappa t)}{8\kappa^4 m t} \right). \quad (22)$$

It is easily verified by straightforward calculation that,

$$i\hbar \frac{\partial G_\gamma(x,t;x',0)}{\partial t} + \frac{\hbar^2}{2m} \frac{\partial^2 G_\gamma(x,t;x',0)}{\partial x^2} = i\hbar \delta(x-x')\delta(t) + \gamma(x-x_c) \sin(\kappa t) G_\gamma(x,t;x',0). \quad (23)$$

For a plane wave of the form $\psi(x,0) = e^{ik(x-x_c)}$ at $t = 0$ entering the cavity, the solution of the Schrödinger equation in the cavity at time t can be obtained from the propagator by integrating over the variable x' at the initial time:

$$\begin{aligned} \psi_\gamma(x,t) &= \int_{-\infty}^{\infty} dx' G_\gamma(x,t;x',0) e^{ik(x'-x_c)} \\ &= \text{Exp} \left(-\frac{i\hbar k^2 t}{2m} + i \left\{ k - \frac{\gamma}{\hbar\kappa} [1 - \cos(\kappa t)] \right\} \right) \\ &\quad \times (x-x_c) + \frac{ik\gamma t}{\kappa m} \left[1 - \frac{\sin(\kappa t)}{\kappa t} \right] \\ &\quad - \frac{i\gamma^2}{8\hbar\kappa^3 m} [6\kappa t - 8\sin(\kappa t) + \sin(2\kappa t)]; \quad (24) \end{aligned}$$

a normalization constant would not be changed. Similar propagators have been used by Scully, Schwinger, and Englert to describe the Stern-Gerlach effect in a static magnetic field [8,10,11]. The propagator introduced in Eq. (21) is one of a class of time-dependent propagators that can be constructed by path-integral methods [12]. A propagator for an electron in a static electric field gradient was first constructed by Kennard [13].

In the present application, the transverse velocities of atoms are small compared to the launch velocity. The launch velocity determines the total amount of time spent in the cavity by an atom. The atoms are narrowly distributed about the launch velocity in the z direction, so the values of the most likely t that occurs in Eq. (24) will be narrowly distributed about a value τ determined by the on-axis Ramsey pulse, $v_0\tau = L$ where L is the cavity length and v_0 is the central velocity at the entry aperture. For a complete half-sine wave pulse on axis, $\kappa\tau = \pi$ and the exponentials in Eq. (24), which are independent of

and x_c , may be simplified to give:

$$\begin{aligned} \psi_\gamma(x,\tau) &= \text{Exp} \left(-\frac{i\hbar k^2 \tau}{2m} + i \left(k - \frac{2\gamma\tau}{\hbar\pi} \right) (x-x_c) \right. \\ &\quad \left. + \frac{ik\gamma\tau^2}{m\pi} - \frac{i3\gamma^2\tau^3}{4\hbar\pi^2 m} \right). \quad (25) \end{aligned}$$

Thus the propagator takes a plane wave into another plane wave at the entry into the drift region, with another phase determined by the kinetic energy of the particle, the wave number, and the field gradient, without changing the plane-wave normalization. The integrations over spatial variables can be performed by completing the squares in the exponents. For example, to illustrate that order of integration is immaterial, a packet such as Eq. (4) is propagated through the cavity by calculating

$$\begin{aligned} &\int dx' G_\gamma(x,\tau;x',0) \phi(x'-x_c,0) \\ &= \frac{1}{\pi^{1/4}} \frac{e^{i(k_0 - 2\gamma\tau/(\hbar\pi))(x-x_c) - i\hbar k_0^2 \tau/(2m)}}{\sqrt{\sigma + i\hbar\tau/(\sigma m)}} \\ &\quad \times e^{-(x-x_c - \hbar k_0 \tau/m + \gamma\tau^2/(m\pi))^2/[2(\sigma^2 + i\hbar\tau/m)]}. \quad (26) \end{aligned}$$

On the other hand if the packet is constructed at the end of the cavity using Eq. (26), precisely the same result is obtained. This justifies extending the range of integration over x' to infinity, since a well-localized packet is small in size relative to the cavity aperture.

After exiting from the cavity, the wave function can be propagated to the end of the drift region with a free-particle propagator obtained from Eqs. (21) and (22) by setting $\gamma = 0$. Thus, without constructing packets,

$$\begin{aligned} \psi(x,\tau+T)|_\gamma &= \int dx' G_{\gamma=0}(x,T;x',0) \psi_\gamma(x',\tau) \\ &= e^{-\frac{i\hbar k^2(\tau+T)}{2m} + i(k - \frac{2\gamma\tau}{\hbar\pi})(x-x_c)} \\ &\quad \times e^{+\frac{ik\gamma\tau(\tau+2T)}{m\pi} - \frac{i\gamma^2\tau^2(3\tau+8T)}{4\hbar m\pi^2}}. \quad (27) \end{aligned}$$

Such integrals may be performed with the help of a convergence factor [13]; this is discussed in the Appendix.

Concatenation of these propagators can help in understanding the phase factors that enter the calculation. For example, a propagator can be constructed that takes a particle from the entry aperture to the end of the drift region; thus

$$\begin{aligned} G_{\text{free},\gamma,x_c}(x,\tau+T;x',0) &= \int dx'' G_{\gamma=0}(x,T;x'',0) G_\gamma(x'',\tau;x',0) \\ &= \sqrt{\frac{m}{2\pi i\hbar(\tau+T)}} e^{\frac{im(x-x')^2}{2\hbar(\tau+T)} - \frac{i\gamma^2\tau^3(\tau+3T)}{4\hbar m\pi^2(\tau+T)}} e^{-\frac{i\gamma\tau[\tau(x-2x_c+x')+2T(x'-x_c)]}{\hbar\pi(\tau+T)}}. \quad (28) \end{aligned}$$

Propagation from the end of the drift region to the detector, through a cavity with a field gradient γ_p with a packet centered at x_p upon entry, can be calculated with a propagator similar to that in Eq. (28):

$$G_{\text{free},\gamma_p,x_p}(x,\tau+T_d;x',0). \quad (29)$$

Then concatenating these two propagators will take an incoming plane wave all the way to the detector:

$$\begin{aligned}
 G_{\text{final}}(x, 2\tau + T + T_d; x', 0) &= \int dx'' G_{\text{free}, \gamma_p, x_p}(x, \tau + T_d; x'', 0) \\
 &\quad \times G_{\text{free}, \gamma, x_c}(x'', \tau + T, x', 0) \\
 &= \sqrt{\frac{m}{2\pi i \hbar T_t}} e^{\frac{im(x-x')^2}{2\hbar T_t} - \frac{i\gamma\gamma_p\tau^3(\tau+2T_d)}{\hbar m\pi^2 T_t}} \\
 &\quad \times e^{-\frac{i\gamma^2\tau^3(4\tau+3T+3T_d)}{4\hbar m\pi^2 T_t} - \frac{i\gamma_p^2\tau^2(4\tau^2+3\tau T+11\tau T_d+8TT_d)}{4\hbar m\pi^2 T_t}} \\
 &\quad \times e^{-\frac{i\gamma\tau[-2(T+T_d)(x_c-x')+\tau(x-4x_c+3x')]}{\hbar\pi T_t}} \\
 &\quad \times e^{-\frac{i\gamma_p\tau[2T(x-x_p)+\tau(3x-4x_p+x')+2T_d(-x_p+x')]}{\hbar\pi T_t}}, \quad (30)
 \end{aligned}$$

where

$$T_t = 2\tau + T + T_d. \quad (31)$$

Then if we insert the initial plane wave (centered at x_c), at the detector we find the plane wave

$$\begin{aligned}
 \int dx'' G_{\text{final}}(x, 2\tau + T + T_d; x'', 0) e^{ik(x''-x_c)} &= e^{-\frac{i\hbar k^2(T_t)}{2m} + i(k - \frac{2\gamma\tau}{\hbar\pi})(x-x_c) - \frac{2i\gamma_p\tau(x-x_p)}{\hbar\pi}} \\
 &\quad \times e^{\frac{ik\gamma_p\tau(\tau+2T_d)}{m\pi} + \frac{ik\gamma\tau(3\tau+2T+2T_d)}{m\pi} - \frac{2i\gamma\gamma_p\tau^2(\tau+2T_d)}{\hbar m\pi^2}} \\
 &\quad \times e^{-\frac{i\gamma^2\tau^2(11\tau+8T+8T_d)}{4\hbar m\pi^2} - \frac{i\gamma_p^2\tau^2(3\tau+8T_d)}{4\hbar m\pi^2}}. \quad (32)
 \end{aligned}$$

Of course this is only part of the solution since it accounts only for the dynamical particle motion. The internal states of the spinors will be treated in the next section. To compress the equations we write the exponential on the right side of Eq. (32) as

$$e^{i\Phi_f(\gamma, \gamma_p)}. \quad (33)$$

The function given by Eq. (33) is an eigenstate of the momentum operator, since operating on Eq. (32) with the momentum operator $i\hbar\partial/\partial x$, the momentum at the detector is

$$\hbar k - \frac{2\gamma\tau}{m} - \frac{2\gamma_p\tau}{m}. \quad (34)$$

Other components of the wave function will differ in the signs of the contributions from γ and γ_p . Plane waves remain plane; the wavefronts acquire no curvature. Thus there is no focusing of these solutions. This is a consequence of the linear approximations for the field gradients in the dynamical equations of motion. We next consider the development of the internal phases of the spinors.

III. BOUNDARY CONDITIONS; SPINOR PHASES

In this section we discuss boundary conditions appropriate for the spinor part of the f_{\pm} functions, given initial preparation of the wave functions in an arbitrary superposition of a and b states. In this section we consider here only the phase development of the spinors due to their internal energy; the dynamical phases have been treated above. This discussion

also applies to boundary conditions on the wave functions at the beginning of the second cavity passage.

Suppose that upon first entry into the cavity the atomic spinor is in an arbitrary superposition of hyperfine states:

$$\left[\begin{array}{c} e^{-i\theta_1/2} D_a \\ e^{i\theta_1/2} D_b \end{array} \right] \Big|_{t=0} = \left[\begin{array}{c} u_{a0} \\ u_{b0} \end{array} \right]. \quad (35)$$

Solving for the amplitudes D_a and D_b [Eq. (9)] and substituting into Eq. (12) gives initial conditions for f_{\pm} :

$$f_{\pm}(0) = \frac{1}{\sqrt{2}} (u_{a0} e^{i\theta_1/2} \pm u_{b0} e^{-i\theta_1/2}) e^{ik(x'-x_c)}, \quad (36)$$

where x' has been inserted in place of x in anticipation of an integration. If we were to assume the atoms are prepared in the lower hyperfine state before entering the first cavity, then $u_{a0} = 0$ and $u_{b0} = 1$ so the boundary condition Eq. (36) would become

$$f_{\pm}(0) = \pm \frac{1}{\sqrt{2}} (e^{-i\theta_1/2}) e^{ik(x'-x_c)}. \quad (37)$$

Combining Eqs. (9) and (37) in the general case, at the end of the first cavity passage the spinor functions are:

$$u_a(\tau) = \frac{e^{-i[\omega\tau/2+\theta_1/2+a(\tau)]}}{\sqrt{2}} f_+(0) + \frac{e^{-i[\omega\tau/2+\theta_1/2-a(\tau)]}}{\sqrt{2}} f_-(0); \quad (38)$$

$$u_b(\tau) = \frac{e^{i[\omega\tau/2+\theta_1/2-a(\tau)]}}{\sqrt{2}} f_+(0) - \frac{e^{i[\omega\tau/2+\theta_1/2+a(\tau)]}}{\sqrt{2}} f_-(0). \quad (39)$$

In the drift region the spinor states acquire additional phase factors due to their internal energy. These phase factors are respectively

$$e^{\mp i\Delta T/2}. \quad (40)$$

Thus the spinor wave functions at the end of the drift region can be expressed as

$$\begin{aligned}
 u_a(\tau + T) &= \frac{e^{-i(\omega\tau+\Delta T+\theta_1)/2-ia}}{2} (u_{a0} e^{i\theta_1/2} + u_{b0} e^{-i\theta_1/2}) \\
 &\quad + \frac{e^{-i(\omega\tau+\Delta T+\theta_1)/2+ia}}{2} (u_{a0} e^{i\theta_1/2} - u_{b0} e^{-i\theta_1/2}); \quad (41)
 \end{aligned}$$

$$\begin{aligned}
 u_b(\tau + T) &= \frac{e^{i(\omega\tau+\Delta T+\theta_1)/2-ia}}{2} (u_{a0} e^{i\theta_1/2} + u_{b0} e^{-i\theta_1/2}) \\
 &\quad - \frac{e^{i(\omega\tau+\Delta T+\theta_1)/2+ia}}{2} (u_{a0} e^{i\theta_1/2} - u_{b0} e^{-i\theta_1/2}). \quad (42)
 \end{aligned}$$

The signs of γ and $a(\tau)$ occur in a given term with opposite signs, thus at the end of the calculation the dynamical phase factors can be matched with the spinor phase factors.

In Eq. (36), linear combinations of the spinor wave functions are combined to give boundary conditions for the decoupled functions f_{\pm} . Similarly, linear combinations of Eqs. (41) and (42) give boundary conditions for solution of

the decoupled wave equations for second cavity passage. In the second cavity, the phase factor $\exp(\pm i\theta_1/2)$ is replaced by $\exp(\pm i\theta_2/2)$; the value of θ_2 will be discussed in Sec. VIII.

In order to simplify further development, to form the needed combinations we depart from a general treatment and assume the spinors are prepared in the lower hyperfine state, so $u_{a0} = 0$, $u_{b0} = 1$. We therefore need the following linear combinations:

$$u_a(\tau + T)e^{i\theta_2/2} + u_b(\tau + T)e^{-i\theta_2/2} \\ = (\cos \Theta)e^{-ia-i\theta_1/2} + (+i \sin \Theta)e^{-ia-i\theta_1/2}, \quad (43)$$

$$u_a(\tau + T)e^{i\theta_2/2} - u_b(\tau + T)e^{-i\theta_2/2} \\ = -(-i \sin \Theta)e^{ia-i\theta_1/2} - (-\cos \Theta)e^{ia-i\theta_1/2}, \quad (44)$$

$$u_a(2\tau + T + T_d) = \frac{e^{-i(\omega\tau + \Delta T_d)/2 - i\theta_1/2 - i\theta_2/2}}{2} (e^{-ia_p - ia}(\cos \Theta) + e^{ia_p - ia}(i \sin \Theta) + e^{-ia_p + ia}(-i \sin \Theta) + e^{ia_p + ia}(-\cos \Theta)); \quad (46)$$

$$u_b(2\tau + T + T_d) = \frac{e^{i(\omega\tau + \Delta T_d)/2 - i\theta_1/2 + i\theta_2/2}}{2} (e^{-ia_p - ia}(\cos \Theta) + e^{ia_p - ia}(-i \sin \Theta) + e^{-ia_p + ia}(-i \sin \Theta) - e^{ia_p + ia}(-\cos \Theta)). \quad (47)$$

The spinor components in Eqs. (46) and (47) are listed in the order $(\gamma, \gamma_p), (\gamma, -\gamma_p), (-\gamma, \gamma_p), (-\gamma, -\gamma_p)$ corresponding to $(a, a_p), (a, -a_p), (-a, a_p), (-a, -a_p)$.

With the solution for the dynamical phase given in Eq. (33), the wave functions at the detector can now be assembled:

$$u_a(2\tau + T + T_d) = \frac{e^{-i(\omega\tau + \Delta T_d)/2 - i\theta_1/2 - i\theta_2/2}}{2} (e^{-ia_p - ia + i\Phi_f(\gamma, \gamma_p)}(\cos \Theta) + e^{ia_p - ia + i\Phi_f(\gamma, -\gamma_p)}(i \sin \Theta) \\ + e^{-ia_p + ia + i\Phi_f(-\gamma, \gamma_p)}(-i \sin \Theta) + e^{ia_p + ia + i\Phi_f(-\gamma, -\gamma_p)}(-\cos \Theta)); \quad (48)$$

$$u_b(2\tau + T + T_d) = \frac{e^{i(\omega\tau + \Delta T_d)/2 - i\theta_1/2 + i\theta_2/2}}{2} (e^{-ia_p - ia + i\Phi_f(\gamma, \gamma_p)}(\cos \Theta) + e^{ia_p - ia + i\Phi_f(\gamma, -\gamma_p)}(-i \sin \Theta) \\ + e^{-ia_p + ia + i\Phi_f(-\gamma, \gamma_p)}(-i \sin \Theta) + e^{ia_p + ia + i\Phi_f(-\gamma, -\gamma_p)}(+\cos \Theta)). \quad (49)$$

Equations (48) and (49) provide the complete solution for plane-wave spinors passing through the apparatus. In the next section we discuss the dynamical phases arising from transverse particle motion.

IV. CONSTRUCTION OF WAVE PACKETS

We construct wave packets at the detector by multiplying by the weighting function $\exp(-\sigma^2(k - k_0)^2/2)$, as in Eq. (4), and integrating over k . Every term in Eqs. (48) and (49) acquires a normalization factor:

$$N_p = \frac{1}{\sqrt{\sqrt{\pi}(\sigma + \frac{i\hbar T_t}{\sigma m})}}. \quad (50)$$

The expressions become quite cumbersome. We shall illustrate the result in only one case, the first term in Eq. (48). The terms in the exponent involving the wave vector k are

$$-\sigma^2(k - k_0)^2/2 - \frac{i\hbar k^2 T_t}{2m} + ik(x - x_c) \\ + \frac{ik\gamma_p\tau(\tau + 2T_d)}{m\pi} + \frac{ik\gamma\tau(3\tau + 2T + 2T_d)}{m\pi}. \quad (51)$$

where

$$\Theta = \frac{1}{2}(\theta_2 - \theta_1 - \omega\tau - \Delta T). \quad (45)$$

The Ramsey fringe is determined by Θ , which depends on the time τ through the first cavity and T through the drift region.

Equations (41) and (42) give the spinors at the entry to the second cavity in terms of their initial values. Equations of the same form must hold for the spinors at the detector in terms of their values at the entry to the second cavity. Thus the spinors at the detector can be obtained by iterating Eqs. (41) and (42). Such initial values have been given in Eqs. (43) and (44). Therefore we can immediately write down the spinors at the detector. The principal changes are: γ and a are replaced by γ_p and a_p , respectively, θ_1 is replaced by θ_2 , and T is replaced by T_d . Thus at the detector we have

This term then becomes

$$\frac{N_p}{2} e^{-ia_p - ia + i\Phi_{\text{packet}}(k_0, \gamma, \gamma_p)}(\cos \Theta), \quad (52)$$

where

$$\Phi_{\text{packet}}(k_0, \gamma, \gamma_p) \\ = -\frac{\hbar k_0^2 T_t}{2m} - \frac{2\gamma\tau}{\hbar\pi}(x - x_c) \\ - \frac{2\gamma_p\tau}{\hbar\pi}(x - x_p) - \frac{2\gamma\gamma_p\tau^2(\tau + 2T_d)}{4\hbar m\pi^2} \\ + k_0 \left(x - x_c + \frac{\gamma\tau(3\tau + 2T + T_d)}{m\pi} + \frac{\gamma_p\tau(\tau + 2T_d)}{m\pi} \right) \\ + i \frac{(x - x_c - \frac{\hbar k_0 T_t}{m} + \frac{\gamma\tau(3\tau + 2T + 3T_d)}{m\pi} + \frac{\gamma_p\tau(\tau + 2T_d)}{m\pi})^2}{2(\sigma^2 + i\hbar T_t/m)}. \quad (53)$$

The quadratic term in $(x - x_c \dots)^2$ in Eq. (53) clearly shows where the packet is centered. We can also backtrack and obtain the packet center at the exit aperture by setting $T_d = 0$.

The packets for the hyperfine states at the detector are therefore:

$$\begin{aligned} \Psi_a(2\tau + T + T_d) = & \frac{N_p}{2} \times (e^{-ia_p - ia + i\Phi_{\text{packet}}(k_0, \gamma, \gamma_p)}(\cos \Theta) + e^{ia_p - ia + i\Phi_{\text{packet}}(k_0, \gamma, -\gamma_p)}(i \sin \Theta) \\ & + e^{-ia_p + ia + i\Phi_{\text{packet}}(k_0, -\gamma, \gamma_p)}(-i \sin \Theta) + e^{ia_p + ia + i\Phi_{\text{packet}}(k_0, -\gamma, -\gamma_p)}(-\cos \Theta)); \end{aligned} \quad (54)$$

$$\begin{aligned} \Psi_b(2\tau + T + T_d) = & \frac{N_p}{2} \times (e^{-ia_p - ia + i\Phi_{\text{packet}}(k_0, \gamma, \gamma_p)}(\cos \Theta) + e^{ia_p - ia + i\Phi_{\text{packet}}(k_0, \gamma, -\gamma_p)}(-i \sin \Theta) \\ & + e^{-ia_p + ia + i\Phi_{\text{packet}}(k_0, -\gamma, \gamma_p)}(-i \sin \Theta) + e^{ia_p + ia + i\Phi_{\text{packet}}(k_0, -\gamma, -\gamma_p)}(+\cos \Theta)). \end{aligned} \quad (55)$$

To save writing, we shall refer to these terms in order as $\psi_{1a}, \psi_{2a}, \dots, \psi_{3b}, \psi_{4b}$, respectively. The probability of finding a particle in the upper hyperfine state at the detector will be

$$\langle |\Psi_a|^2 \rangle, \quad (56)$$

where $\langle \rangle$ means appropriately averaged over thermal velocities and integrated over the apertures.

In computing probabilities such as in Eq. (56), each of the squared terms gives 16 contributions. The forms for the solutions given above allow us to cancel many terms even without knowing much about the functions Φ_{packet} . We are going to compress the notation by labeling the terms in the solutions with subscripts 1 through 4. Thus for example, for the contribution from the square of the lower hyperfine state, the product of the first term, times the complex conjugate of the third term, will be denoted by

$$ie^{-2ia} \cos \Theta \sin \Theta P_{13b} = N_p^2 \int \langle (\cos \Theta e^{-ia - ia_p} e^{i\Phi_{\text{packet}}(\gamma, \gamma_p)})(i \sin \Theta e^{-ia + ia_p} e^{i\Phi_{\text{packet}}^*(-\gamma, \gamma_p)}) \rangle. \quad (57)$$

Then normalization of the wave function at the detector is computed by means of

$$\begin{aligned} \int \langle |\Psi_a|^2 \rangle = & \frac{1}{4} ((\cos \Theta)^2 (P_{11a} + P_{44a}) - (\cos \Theta)^2 (e^{-2ia_p - 2ia} P_{14a} + e^{2ia_p + 2ia} P_{41a}) + (\sin \Theta)^2 (P_{22a} + P_{33a}) \\ & - (\sin \Theta)^2 (e^{2ia_p - 2ia} P_{23a} + e^{-2ia_p + 2ia} P_{32a}) + i \cos \Theta \sin \Theta (-e^{-2ia_p} P_{12a} + e^{2ia_p} P_{21a} + e^{-2ia} P_{13a} - e^{2ia} P_{31a} \\ & - e^{-2ia} P_{24a} + e^{2ia} P_{42a} + e^{-2ia_p} P_{34a} - e^{2ia_p} P_{43a})), \end{aligned} \quad (58)$$

and

$$\begin{aligned} \int \langle |\Psi_b|^2 \rangle = & \frac{1}{4} ((\cos \Theta)^2 (P_{11b} + P_{44b}) + (\cos \Theta)^2 (e^{-2ia_p - 2ia} P_{14b} + e^{2ia_p + 2ia} P_{41b}) + (\sin \Theta)^2 (P_{22b} + P_{33b}) \\ & + (\sin \Theta)^2 (e^{2ia_p - 2ia} P_{23b} + e^{-2ia_p + 2ia} P_{32b}) + i \cos \Theta \sin \Theta (-e^{-2ia_p} P_{12b} - e^{2ia_p} P_{21b} + e^{-2ia} P_{13b} - e^{2ia} P_{31b} \\ & - e^{-2ia} P_{24b} + e^{2ia} P_{42b} - e^{-2ia_p} P_{34b} + e^{2ia_p} P_{43b})). \end{aligned} \quad (59)$$

These integrals have been defined so that when “ \int ” in Eqs. (58) or (59) is interpreted as an integration over all space,

$$P_{iaa} = P_{iib} = 1, \quad i = 1, 2, 3, 4. \quad (60)$$

It can then be shown that for all i and j ,

$$P_{ija} = P_{ijb}. \quad (61)$$

The normalization condition reduces to

$$1 = 1 + \frac{2}{4} i \cos \Theta \sin \Theta \int (e^{-2ia} P_{13a} - e^{2ia} P_{31a} - e^{-2ia} P_{24a} + e^{2ia} P_{42a}). \quad (62)$$

In can be shown that in addition to the above symmetry properties of the integrals, we have when integrating over all space

$$P_{13a} = P_{24a}; \quad P_{31a} = P_{42a}. \quad (63)$$

Therefore all terms proportional to $\cos \Theta \sin \Theta$ on the right side of the normalization condition cancel and the solution is correctly normalized. In order for the integrals to converge, it is necessary to construct wave packets as in Eq. (4) before squaring.

V. PACKET CENTERS

The factors multiplying the terms in large parentheses in Eqs. (48) and (49) cannot affect any probability computed

from the squares of the wave functions; these factors will therefore be dropped.

Wave packets can be constructed at the beginning or end of the drift region by taking weighted superpositions of

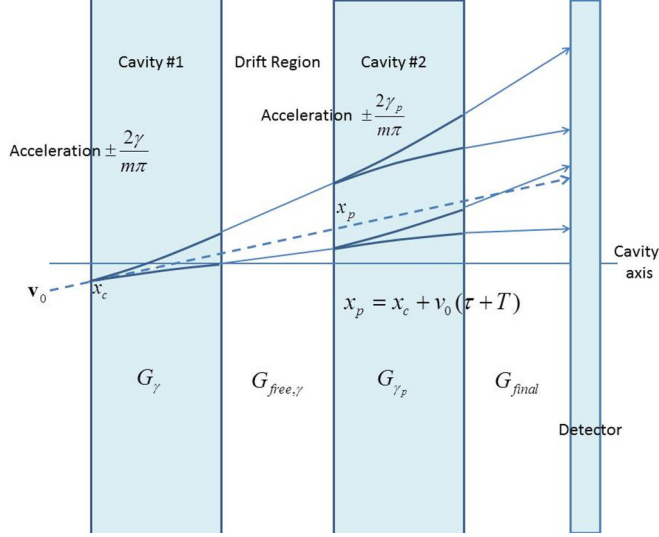


FIG. 2. (Color online) Schematic illustration of trajectories of packets through the system; each cavity causes separation into two packets, each with equal numbers of a and b spinor states. The ordinate represents the direction transverse to the cavity axis. G_{free} is defined in (23); $G_{\text{free},\gamma}$ is defined in (28), and G_{final} is defined in (30).

$e^{ik(x-x_c)}$ as in Eq. (4). Figure 2 illustrates, greatly exaggerated, what happens to the wave packet trajectories. The decoupled components travel in opposite directions in the first cavity, with an effective acceleration $\pm 2\gamma/(m\pi)$. For a typical off-axis field gradient, the separation in position is only about a nanometer. The velocity difference is about 15 nm/s, so at the end of the drift region if $T = 1$ s, the packet separation is only about 30 nm. On the other hand a typical transverse velocity due to a finite temperature of $\approx 0.5 \mu\text{K}$ is 0.008 m/sec. The displacements due to the thermal velocity distribution are $\approx 3 \times 10^5$ larger than the displacements due to transverse field gradients. The latter are also small on the scale of changes in the transverse field gradients themselves. We therefore use a value of γ , denoted by γ_p , in the second cavity that accounts for the change in the central position of the packet during time $\tau + T$. A packet entering the first cavity with position x_c and average velocity $\hbar k_{0x}/m$ will end up, on average, at the entry to the second cavity with position

$$x_p = x_c + \hbar k_{0x}(\tau + T)/m. \quad (64)$$

The field gradient at this position will be denoted by

$$\begin{aligned} \gamma_p &= -\frac{\hbar\pi b x_1^2 x_p}{4d^2} \\ &= -\left(\frac{\hbar\pi b x_1^2 x_c}{4d^2} + \frac{\hbar^2\pi b x_1^2 k_{0x}(\tau + T)}{4d^2 m}\right), \end{aligned} \quad (65)$$

and the second term will be accounted for when performing thermal averages. On exiting the first cavity, the packet will be centered at

$$x = x_c + \frac{\hbar k_{0x}\tau}{m} \mp \frac{\gamma\tau^2}{m\pi}; \quad (66)$$

at the end of the drift region, the center will be at

$$x = x_c + \frac{\hbar k_{0x}(\tau + T)}{m} \mp \frac{\gamma\tau(\tau + 2T)}{m\pi}; \quad (67)$$

after exiting from the second cavity, the center will be at

$$x = x_c + \frac{\hbar k_{0x}(2\tau + T)}{m} \mp \frac{\gamma\tau(3\tau + 2T)}{m\pi} \mp \frac{\gamma_p\tau^2}{m\pi}; \quad (68)$$

and finally at the detector the center will be

$$\begin{aligned} x = x_c + \frac{\hbar k_{0x}(2\tau + T + T_d)}{m} \mp \frac{\gamma\tau(3\tau + 2T + 2T_d)}{m\pi} \\ \mp \frac{\gamma_p\tau(\tau + 2T_d)}{m\pi}. \end{aligned} \quad (69)$$

The parameter $a_p(\tau)$ in the second cavity will also be affected by transverse forces. If the on-axis value of $a(\tau)$ is given by a normal $\pi/2$ pulse, then for an atom on the axis,

$$a_{\text{axis}} = b\tau = \pi/4. \quad (70)$$

At the entry to the first cavity we have

$$a = a_{\text{axis}} \left(1 - \frac{x_1^2 x_c^2}{4d^2}\right), \quad (71)$$

and therefore at the entry to the second cavity

$$a_p = a_{\text{axis}} \left(1 - \frac{x_1^2 [x_c + \hbar k_{0x}(\tau + T)/m]^2}{4d^2}\right). \quad (72)$$

VI. LAUNCH CONDITIONS, THERMAL AVERAGING

In NIST-F2, atoms are collected, cooled, and launched from a trap some dozens of centimeters below the cavity entry aperture. We let $z_L < 0$, $v_L > 0$ and $t_L < 0$ be the launch position, velocity and time of launch, such that the atom clouds are centered at the entry aperture at $z = 0$, $t = 0$ with entry velocity $v_0 = v_L + g t_L$. Here z is positive upwards and the acceleration of gravity is $-g$. We treat the cloud of atoms as collisionless, characterized by an initial spread σ_n and temperature T_n in the transverse directions, and spread σ_p and temperature T_p in the z dimension. The atom distribution is described by a product of exponential distribution functions of the following form:

$$f_n(x, v_x, t) = \frac{1}{2\pi\sigma_n} \sqrt{\frac{m}{k_B T_n}} e^{-\frac{(x-v_x(t+t_L))^2}{2\sigma_n^2}} e^{-\frac{mv_x^2}{2k_B T_n}}, \quad (73)$$

$$\begin{aligned} f_p(z, v_z, t) = \frac{1}{2\pi\sigma_p} \sqrt{\frac{m}{k_B T_p}} e^{-\frac{m(v_z - v_L + g(t+t_L))^2}{2k_B T_p}} \\ \times e^{-\frac{(z+d_L - v_z(t+t_L) - g(t+t_L))^2/2}{2\sigma_p^2}}. \end{aligned} \quad (74)$$

Then the complete distribution function is

$$f(\mathbf{r}, \mathbf{v}, t) = f_n(x, v_x, t) f_n(y, v_y, t) f_p(z, v_z, t). \quad (75)$$

This distribution function satisfies the collisionless Boltzmann equation,

$$\frac{\partial f}{\partial t} + \mathbf{v} \cdot \nabla f - g \frac{\partial f}{\partial z} = 0. \quad (76)$$

At $t = t_L$, the cloud is centered at $z = z_L$. In the transverse direction, the half-width of the cloud is σ_n at $t = -t_L$ (in a single transverse dimension) and spreads to $[\sigma_n^2 + k_B(t + t_L)^2 T_n/m]^{1/2}$ after time t .

There are many contributions to the width of the wave packets and to the atom balls; generally these combine in quadrature. First, there is the initial half-width σ at launch, which is not known precisely. Due to quantum-mechanical spreading of a packet, there is a second contribution to the half-width that increases with time but is inversely proportional to σ . If σ is small, quantum mechanical spreading will become large and contribute significantly to clipping. The value of σ has been set equal to the approximate thermal wavelength of a Cs¹³³ atom, about 200 nm. In Fig. 9 we illustrate the effect of changing this assumption, and verify that the results do not depend significantly on the choice of this parameter. Third, there is a contribution arising from thermal averaging over the transverse velocities. At temperatures 0.5 μ K and higher, and after a Ramsey time in the neighborhood of 1 s, this contribution dominates the spreading of the ball. There are numerous additional contributions to spreading, of the order of a nanometer or less, arising from transverse field gradients and off-axis positions of the atoms. These contributions are automatically included in the calculations.

VII. ONE-DIMENSIONAL MODEL

The detector measures the numbers of particles in the cloud in each of the hyperfine states and the following ratio is computed:

$$\frac{\int \langle |\Psi_a|^2 \rangle}{\int \langle |\Psi_a|^2 \rangle + \int \langle |\Psi_b|^2 \rangle}, \quad (77)$$

where the integrals go over the initial aperture with a weight function determined by the Boltzmann distribution, after forming wave packets. Thus we average with

$$\int_{-D/2}^{D/2} f_n(x_c, v_x, 0) dx_c dv_x |\Psi(x)|^2, \quad (78)$$

where $D = .005$ meters is the aperture radius. We also integrate over the exit aperture:

$$\int \langle |\Psi_a|^2 \rangle = \int_{-D/2}^{D/2} dx \int_{-D/2}^{D/2} f_n(x_c, v_x, 0) dx_c dv_x |\Psi_a(x)|^2 \quad (79)$$

with the understanding that the integrals now go over a finite region, we still denote the contributions with notations such as P_{11a} , etc. The dependence of the spinor part of the wave functions is not affected by such restrictions.

The numerator of Eq. (77) is of the form

$$\int \langle |\Psi_a|^2 \rangle = A_a + B_a \cos 2\Theta + C_a \sin 2\Theta, \quad (80)$$

where

$$A_a = \frac{1}{8}(P_{11a} + P_{22a} + P_{33a} + P_{44a} - e^{-2ia_p - 2ia} P_{14a} - e^{2ia_p + 2ia} P_{41a} - e^{2ia_p - 2ia} P_{23a} - e^{-2ia_p + 2ia} P_{32a}), \quad (81)$$

$$B_a = \frac{1}{8}(P_{11a} - P_{22a} - P_{33a} + P_{44a} - e^{-2ia_p - 2ia} P_{14a} - e^{2ia_p + 2ia} P_{41a} + e^{2ia_p - 2ia} P_{23a} + e^{-2ia_p + 2ia} P_{32a}), \quad (82)$$

$$C_a = \frac{i}{8}(-e^{-2ia_p} P_{12a} + e^{2ia_p} P_{21a} + e^{-2ia} P_{13a} - e^{2ia} P_{31a} - e^{-2ia} P_{24a} + e^{2ia} P_{42a} + e^{-2ia_p} P_{34a} - e^{2ia_p} P_{43a}). \quad (83)$$

Similarly for the other hyperfine state,

$$A_b = \frac{1}{8}(P_{11b} + P_{22b} + P_{33b} + P_{44b} + e^{-2ia_p - 2ia} P_{14b} + e^{2ia_p + 2ia} P_{41b} + e^{2ia_p - 2ia} P_{23b} + e^{-2ia_p + 2ia} P_{32b}), \quad (84)$$

$$B_b = \frac{1}{8}\left(P_{11b} - P_{22b} - P_{33b} + P_{44b} + e^{-2ia_p - 2ia} P_{14b} + e^{2ia_p + 2ia} P_{41b} - e^{2ia_p - 2ia} P_{23b} - e^{-2ia_p + 2ia} P_{32b}\right), \quad (85)$$

$$C_b = \frac{i}{8}(e^{-2ia_p} P_{12b} - e^{2ia_p} P_{21b} + e^{-2ia} P_{13b} - e^{2ia} P_{31b} - e^{-2ia} P_{24b} + e^{2ia} P_{42b} - e^{-2ia_p} P_{34b} + e^{2ia_p} P_{43b}). \quad (86)$$

The denominator of Eq. (77) is the sum of contributions from both hyperfine states and is therefore

$$A + B \cos 2\Theta + C \sin 2\Theta, \quad (87)$$

where

$$A = A_a + A_b = \frac{1}{4}(P_{11a} + P_{22a} + P_{33a} + P_{44a}); \quad (88)$$

$$B = B_a + B_b = \frac{1}{4}(P_{11a} - P_{22a} - P_{33a} + P_{44a});$$

$$C = C_a + C_b = \frac{i}{4}(e^{-2ia} P_{13a} - e^{2ia} P_{31a} - e^{-2ia} P_{24a} + e^{2ia} P_{42b}). \quad (89)$$

and where we have made use of the relations Eqs. (60) and (61).

VIII. DETECTION

Let the numbers of particles detected in the a and b hyperfine states be

$$n_a = \left\langle \int |\Psi_a|^2 \right\rangle; \quad (90)$$

$$n_b = \left\langle \int |\Psi_b|^2 \right\rangle, \quad (91)$$

where it is understood that the spatial integrals go only over the apertures, and that averages over transverse velocity are performed with weight functions derived from Eq. (75).

The transition probabilities found in the preceding calculations depend on the phase difference $\theta_2 - \theta_1$ only through the quantity

$$2\Theta = \theta_2 - \theta_1 - (\omega\tau + \Delta T). \quad (92)$$

At the instant the atom enters the cavity for the second time, the angle θ_2 includes the advance of phase of the microwave field, as well as any additional phase angle α that is imposed on

the rf field during the drift time. Thus at resonance the phase of the microwave field satisfies

$$\begin{aligned}\theta_2 &= \theta_1 + \omega(\tau + T) + \alpha; \\ 2\Theta &= \alpha + (\omega - \Delta)T.\end{aligned}\quad (93)$$

Due to the contributions of the coefficients C_a, C_b to the transition probabilities, the center of the line will be slightly shifted from its nominal value at $\omega = \Delta$.

In the F-2 fountain, the central Ramsey fringe is located, corresponding ideally to $\alpha = 0$, $\omega = \Delta$. The numbers of particles in the upper hyperfine state are measured part way down the line profile, on opposite sides of the line in successive balls; this corresponds to setting $(\omega - \Delta)T = \pm\pi/2$, or, if $\omega = \Delta$, $\alpha = \pm\pi/2$. A servo locates the line center in such a way that the numbers observed on the two sides of the line are equal. A frequency-shift error $\delta\omega$ would appear through an additional term $\Delta \rightarrow \Delta + \delta\omega$ in Eq. (93):

$$2\Theta_{\pm} = \pm\pi/2 - \delta\omega T. \quad (94)$$

After thermal averages and averages over the aperture are taken, theory gives the following predictions for the observables:

$$\left. \frac{n_+}{n_+ + n_-} \right|_{+\alpha} = \frac{A_a + B_a \cos(2\Theta_+) + C_a \sin(2\Theta_+)}{A + B \cos(2\Theta_+) + C \sin(2\Theta_+)}; \quad (95)$$

$$\left. \frac{n_+}{n_+ + n_-} \right|_{-\alpha} = \frac{A_a + B_a \cos(2\Theta_-) + C_a \sin(2\Theta_-)}{A + B \cos(2\Theta_-) + C \sin(2\Theta_-)}. \quad (96)$$

If the coefficients C_a, C_b vanish and the remaining coefficients are finite, there could be no frequency shift since the transition probabilities would be symmetric with respect to reflection about the line center.

We consider two cases. First, setting the ratios in Eqs. (95) and (96) equal, expanding for small $\delta\omega$ and solving we find that $\delta\omega$ is proportional to the factor

$$\cos(\alpha)(CB_a - BC_a) - (AC_a - CA_a). \quad (97)$$

If α were chosen to satisfy the above relation, the shift of the center of the line would be unobservable. For NIST-F2, $\alpha \approx 1.7$ radians, whereas the value of α actually used in making measurements is $\pi/2 = 1.57$ radians. Figure 3 shows the calculated shift as a function of the angle α for a reasonable

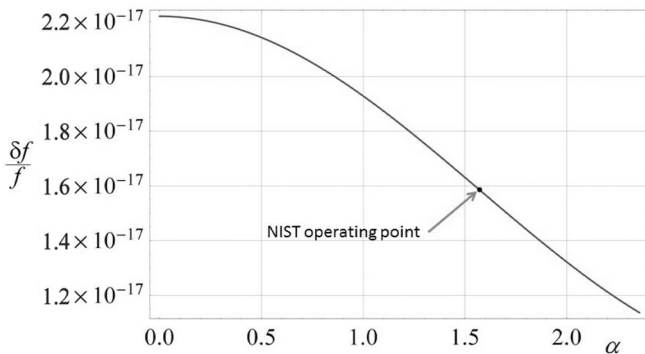


FIG. 3. Calculated fractional frequency shift as a function of the angle α in the two-dimensional case. The values of toss height h and temperature are 1.1 m and $0.5 \mu\text{K}$, respectively.

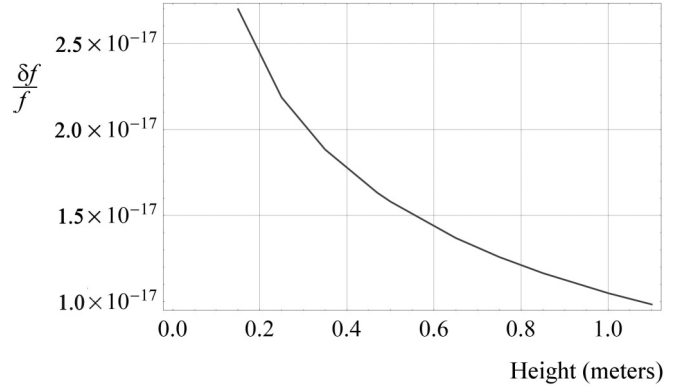


FIG. 4. Fractional shift at temperature $0.5 \mu\text{K}$ as a function of toss height; one-dimensional calculation.

set of parameters. The measured shift decreases from the actual shift at $\alpha = 0$ to a smaller value at $\alpha = \pm\pi/2$.

Second, for the actual operating conditions of NIST-F1 and NIST-F2, $\alpha = \pm\pi/2$. Solving for the shift as in the previous case,

$$\delta\omega = \frac{CA_a - AC_a}{AB_a T}; \quad (98)$$

the fractional-frequency error is thus

$$\frac{\delta\omega}{\omega} = \frac{CA_a - AC_a}{2\pi \times (9.192 \times 10^9 \text{Hz}) AB_a T}. \quad (99)$$

IX. RESULTS: ONE-DIMENSIONAL CASE

Figure 4 plots the fractional-frequency shift as a function of toss height h , at a temperature of $0.5 \mu\text{K}$. The fractional-frequency shift as a function of initial atom cloud temperature is plotted in Fig. 5 for a toss height of 0.75 m.

X. TWO-DIMENSIONAL MODEL

The theory may be extended to two dimensions in a straightforward way. Eq. (19) admits a solution that is a product $\alpha(x,t)\beta(y,t)$. The function β is formally identical to α with replacements $x \rightarrow y$, $x_c \rightarrow y_c$, $\gamma_x \rightarrow \gamma_y$, $x_p \rightarrow y_p$, $\gamma_{xp} \rightarrow \gamma_{yp}$, $k_0 = k_{0x} \rightarrow k_{0y}$, $|N_p|^2 \rightarrow |N_p|^4$. Factors such as

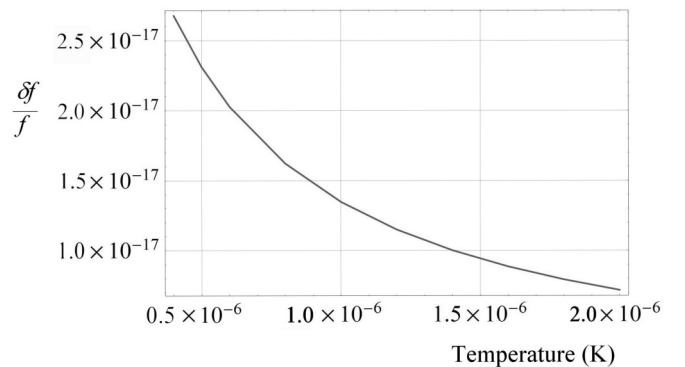


FIG. 5. Fractional frequency shift for various atom cloud temperatures at a toss height of 0.75 meters; one-dimensional calculation.

$e^{\pm ia \pm a_p} \cos(\Theta)$ are formally unchanged, but a and a_p are evaluated at an off-axis point corresponding to (x_c, y_c) . Thus, Eqs. (71) and (72) become

$$a = a_{\text{axis}} \left(1 - \frac{x_1^2(x_c^2 + y_c^2)}{4d^2} \right); \quad (100)$$

$$a_p = a_{\text{axis}} \left(1 - \frac{x_1^2(x_c + \hbar k_{0x}(\tau + T)/m)^2}{4d^2} - \frac{x_1^2(y_c + \hbar k_{0y}(\tau + T)/m)^2}{4d^2} \right). \quad (101)$$

Cavity phase factors involving a and a_p are sums in the exponent, which becomes a product of exponential phase

factors. The dynamical phase factors in Eqs. (54) and (55) are augmented by factors of the form

$$e^{i\Phi_{\text{packet}}(k_{0y}, \pm\gamma_y, \pm\gamma_{yp})}. \quad (102)$$

Let

$$\begin{aligned} \Phi_{pkt}(k_{0x}, \gamma_x, \gamma_{xp}, k_{0y}, \gamma_y, \gamma_{yp}) \\ = \Phi_{\text{packet}}(k_{0x}, \gamma_x, \gamma_{xp}) + \Phi_{\text{packet}}(k_{0y}, \gamma_y, \gamma_{yp}). \end{aligned} \quad (103)$$

(We suppress the dependence on x, x_c, x_p, y, y_c, y_p to save writing.) Then the wave functions at the detector are

$$\begin{aligned} \Psi_a(2\tau + T + T_d) = \frac{N_p^2}{2} (e^{-ia_p - ia + i\Phi_{pkt}(k_{0x}, \gamma_x, \gamma_{xp}, k_{0y}, \gamma_y, \gamma_{yp})} (\cos \Theta) + e^{ia_p - ia + i\Phi_{pkt}(k_{0x}, \gamma_x, -\gamma_{xp}, k_{0y}, \gamma_y, -\gamma_{yp})} (i \sin \Theta) \\ + e^{-ia_p + ia + i\Phi_{pkt}(k_{0x}, -\gamma_x, \gamma_{xp}, k_{0y}, -\gamma_y, \gamma_{yp})} (-i \sin \Theta) + e^{ia_p + ia + i\Phi_{pkt}(k_{0x}, -\gamma_x, -\gamma_{xp}, k_{0y}, -\gamma_y, -\gamma_{yp})} (-\cos \Theta)); \end{aligned} \quad (104)$$

$$\begin{aligned} \Psi_b(2\tau + T + T_d) = \frac{N_p^2}{2} (e^{-ia_p - ia + i\Phi_{pkt}(k_{0x}, \gamma_x, \gamma_{xp}, k_{0y}, \gamma_y, \gamma_{yp})} (\cos \Theta) + e^{ia_p - ia + i\Phi_{pkt}(k_{0x}, \gamma_x, -\gamma_{xp}, k_{0y}, \gamma_y, -\gamma_{yp})} (-i \sin \Theta) \\ + e^{-ia_p + ia + i\Phi_{pkt}(k_{0x}, -\gamma_x, \gamma_{xp}, k_{0y}, -\gamma_y, \gamma_{yp})} (-i \sin \Theta) + e^{ia_p + ia + i\Phi_{pkt}(k_{0x}, -\gamma_x, -\gamma_{xp}, k_{0y}, -\gamma_y, -\gamma_{yp})} (+\cos \Theta)). \end{aligned} \quad (105)$$

The Boltzmann distribution function for motion in the y direction is formally the same as that for motion in the x direction, and the net particle distribution function that depends on x and y is just a product of two similar exponential functions. Similarly, the quantum mechanical probability that depends on the two transverse coordinates (x, y) is just a product of two functions of the same form. If we let P_{ija} or P_{ijb} denote integrals over x as in Eq. (57), and Q_{ija} or Q_{ijb} denote corresponding integrals over y , then Eqs. (58) and (59) are valid when we make the replacements:

$$P_{ija} \rightarrow P_{ija} Q_{ija}; \quad P_{ijb} \rightarrow P_{ijb} Q_{ijb}. \quad (106)$$

The discussion of detection is unchanged.

When numerically averaging over a circular entry aperture, x and y are restricted to

$$(x^2 + y^2)^{1/2} \leq r_a; \quad (x_c^2 + y_c^2)^{1/2} \leq r_a. \quad (107)$$

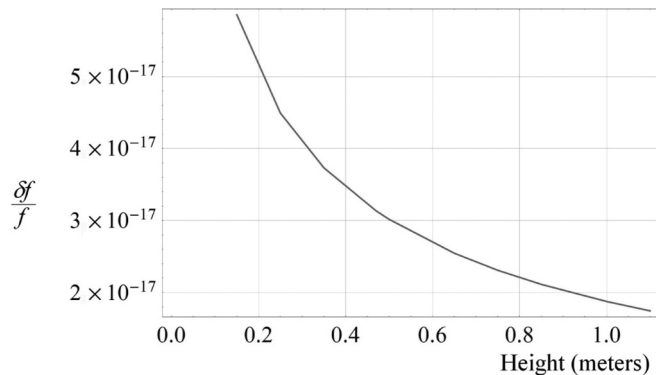


FIG. 6. Fractional frequency shift vs. toss height for NIST-F2 at a temperature of $0.5 \mu\text{K}$; full two-dimensional calculation.

For thermal averaging over the initial velocity distributions, the transverse part of the Boltzmann distribution takes the following two-dimensional form:

$$\begin{aligned} f(x, v_x, y, v_y, 0) = f_n(x, v_x, 0) f_n(y, v_y, 0) \\ = \frac{m}{(2\pi\sigma_n)^2 k_B T} e^{-\frac{m}{2k_B T} (v_x^2 + v_y^2)} e^{-\frac{(x - v_x t_L)^2}{2\sigma_n^2}} \\ \times e^{-\frac{(y - v_y t_L)^2}{2\sigma_n^2}}. \end{aligned} \quad (108)$$

XI. RESULTS: TWO-DIMENSIONAL MODEL

In Fig. 6 we plot the results for transmission through circular apertures of radius 5 mm for temperature $T = 0.5 \mu\text{K}$, as a function of toss height. This should be compared with the one-dimensional results plotted in Fig 3. Figure 7 plots the fractional frequency shift at a fixed height, as a function of the temperature. In Fig. 8 we plot the probability of arrival at the detector, of a state-selected and launched atom, as a

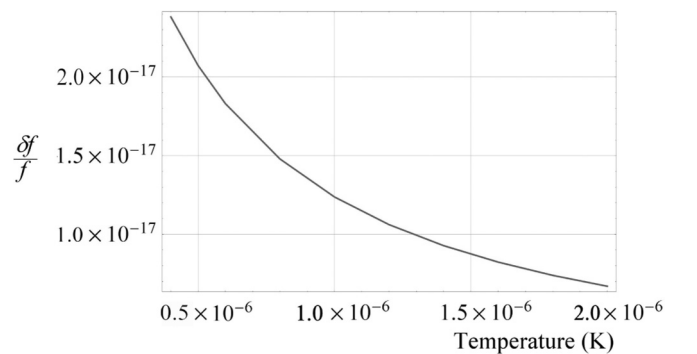


FIG. 7. Fractional frequency shift for NIST-F2 at a toss height of 0.75 m , as a function of temperature.

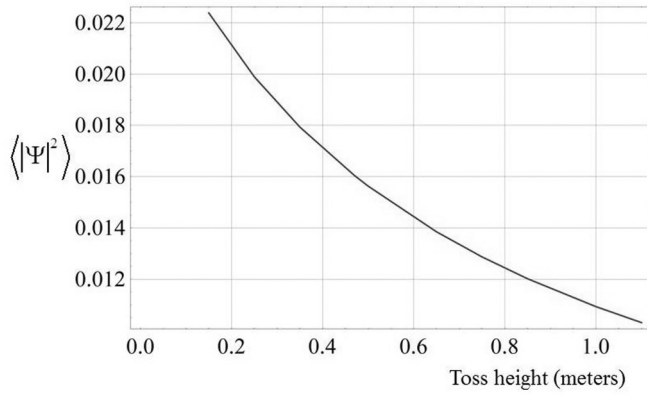


FIG. 8. Fraction of atoms arriving at the detector as a function of toss height; two-dimensional case.

function of toss height. The fraction decreases as toss height increases because the atom ball has more time to spread out due to the distribution of thermal velocities. Figure 9 shows the frequency-shift dependence on initial packet-width for a toss height of 0.47 m at temperature 0.5 μ K. The wave packet widths at launch are unknown; if chosen to be too small, quantum-mechanical spreading will become very important and loss of atoms due to clipping by the apertures will become significant. In Fig. 9 we plot the fractional frequency shift as a function of the width parameter σ . (The one-dimensional de Broglie wavelength of a cesium atom at 0.5 μ K is about 540 nm.) If the assumed width is larger than about 200 nm, which is the value we have used in all our other calculations, the shift is essentially independent of σ . Figure 10 plots the fractional frequency shifts as a function of toss height for NIST-F2 for $\pi/2$, $3\pi/2$, and $5\pi/2$ pulses.

Table I provides values of the fractional frequency shift as a function of rf amplitude corresponding to $b = \pi/4\tau$, $3\pi/4\tau$, $5\pi/4\tau$, and $7\pi/4\tau$ pulses for different toss heights. For $b = 3\pi/4\tau$ and $7\pi/4\tau$, the $n\pi/2$ the shifts are negative. The dependence on applied rf amplitude is similar to that of the microwave leakage frequency shift and is accounted for during normal evaluation of the NIST fountains.

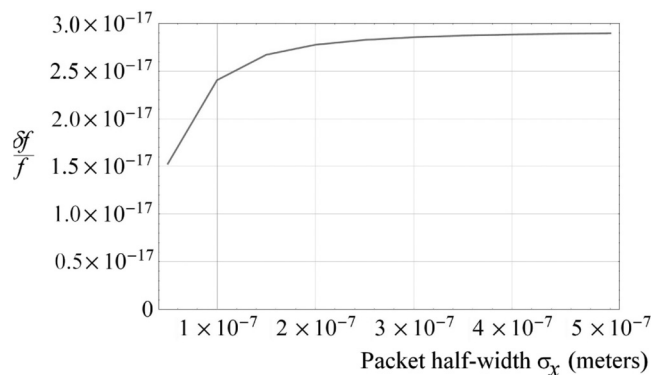


FIG. 9. Fractional frequency shift for a toss height of 0.47 m and a temperature of 0.5 μ K as a function of initial packet width.

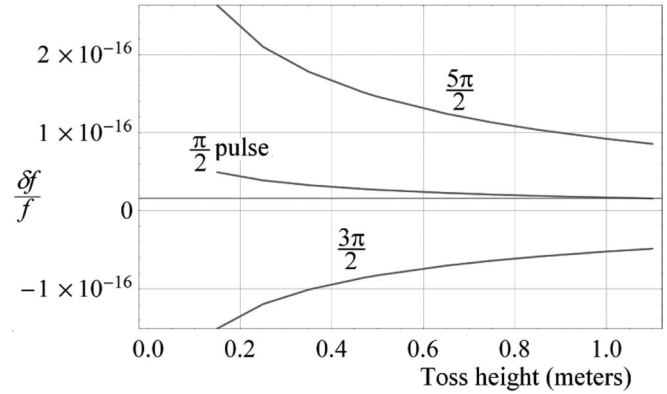


FIG. 10. Fractional frequency shift as a function of toss height for $\pi/2$, $3\pi/2$, $5\pi/2$ pulses.

XII. CONCLUSIONS

For the parameters for NIST-F1 and NIST-F2 cesium fountains, e.g., cavity radius, configuration of detectors, aperture size, etc., we have not found any conditions such that frequency shifts due to transverse field gradients are large enough to be significant in the systematic error budget. We have accounted for many factors that make the present calculation realistic. These include temperature and spatial distributions in the launched atom balls, quantum-mechanical spreading of the atomic wave packets, clipping of probability distributions at aperture boundaries, distances between trapping regions, cavities, and detectors that affect times of passage of atoms through the cavities and the time spent in the drift region, transverse motion of atoms in the drift region that results in their sampling different values of the transverse field gradients, off-axis values of the Rabi pedestal, as well as a full two-dimensional theory of atomic trajectories through the cavities based on an exact Green's function solution of the Schrödinger equation in the presence of a transverse field gradient.

In this approach, the Green's function solutions require integrations from $-\infty$ to $+\infty$ in the transverse direction, whereas such directions are actually limited by the cavity apertures. However, wave packets are concentrated in a very small region and their distributions rapidly approach zero away from their centroids; although contributions to such integrals outside of the apertures are extremely small, they have not been included in the final integrations. The half-sine wave form assumed for the axial component of the magnetic field is an

TABLE I. Fractional shifts $\times 10^{17}$ for various launch heights as a function of applied microwave field amplitude. The last line contains the values extrapolated to zero applied rf amplitude.

b	height(m)		
	0.47	0.75	1.00
$\pi/4\tau$	2.78	2.07	1.69
$3\pi/4\tau$	-8.56	-6.39	-5.22
$5\pi/4\tau$	15.1	11.3	9.20
$7\pi/4\tau$	-23.3	-17.4	-14.2
0 (fit)	-1.2	-0.9	-0.7

approximation; the resulting exponential form of the Green's function allows many propagation integrals to be performed analytically, so that only integrations of the probability densities over the entry and exit apertures are performed numerically. The assumed clipping of the atom wave packets at the aperture walls is an idealization. No theory of the physics of atomic fountains to date, including the theory presented here, has a realistic treatment of the atom-wall interactions.

APPENDIX

The integral, Eq. (29), may be evaluated with the aid of a convergence factor that is allowed to approach zero at the end

of the calculation. Displaying only the factors that participate in the integration, we have

$$\begin{aligned} & \lim_{\alpha \rightarrow 0} \sqrt{\frac{m}{2\pi i \hbar T}} \int dx' e^{\frac{im(x-x')^2}{2\hbar T} - \alpha^2(x-x')^2 + i(k \mp \frac{2\gamma\tau}{\hbar\pi})(x-x')} \\ &= \lim_{\alpha \rightarrow 0} \sqrt{\frac{m}{2\pi i \hbar T}} \sqrt{2\pi} \sqrt{\frac{\hbar T}{-im + 2\alpha^2 \hbar T}} \\ & \quad \times e^{(k \mp \frac{2\gamma\tau}{\hbar\pi})^2 / [2im/(\hbar T) - 2\alpha^2]} \\ &= \exp \left[-i \hbar T \left(k \mp \frac{2\gamma\tau}{\hbar\pi} \right)^2 / (2m) \right]. \end{aligned} \tag{A1}$$

When combined with the other phase factors in Eq. (27) this yields Eq. (30).

[1] R. Wynands and S. Weyers, *Metrologia* **42**, S64 (2005).
 [2] P. Wolf and C. J. Bordé, [arXiv:quant-ph/0403194](https://arxiv.org/abs/quant-ph/0403194).
 [3] R. Li, K. Gibble, and K. Szymaniec, *Metrologia* **48**, 283 (2011).
 [4] K. Gibble, *Phys. Rev. Lett.* **97**, 073002 (2006).
 [5] R. J. Cook, *Phys. Rev. Lett.* **41**, 1788 (1978).
 [6] R. J. Cook, *Phys. Rev. A* **35**, 3844 (1987).
 [7] T. P. Heavner, S. R. Jefferts, E. A. Donley, J. H. Shirley, and T. E. Parker, *Metrologia* **42**, 411 (2005).
 [8] M. O. Scully, B.-G. Englert, and J. Schwinger, *Phys. Rev. A* **40**, 1775 (1989).
 [9] J. H. Shirley, W. D. Lee, and R. E. Drullinger, *Metrologia* **38**, 427 (2001).
 [10] J. Schwinger, M. O. Scully, and B.-G. Englert, *Z. Phys. D* **10**, 135 (1988).
 [11] B.-G. Englert, J. Schwinger, and M. O. Scully, *Found. Phys.* **18**, 1045 (1988).
 [12] L. S. Shulman, *Techniques and Applications of Path-Integral Methods* (Wiley, New York, 1981), p. 38.
 [13] E. H. Kennard, *Z. Phys.* **44**, 326 (1927).